Extensive adsorption of the lighter homologue tellurium of polonium from wastewater using porous silver layer deposited stainless steel mesh

Xiaojiao Zhou [a,b,*], Chao Wang [a], Hua Huang [a,**], Xiang Ji [a], Bin Wu [a]

[a] Key Laboratory of Neutronics and Radiation Safety, Institute of Nuclear Energy Safety Technology, Chinese Academy of Science, Hefei 230031, China
[b] University of Science and Technology of China, Hefei 230027, China

ARTICLE INFO

ABSTRACT

Polonium-210 is a key radioactive hazard for accelerator driven sub-critical system, in which the lead-bismuth eutectic is used as coolant and spallation target. To solve its potential pollution problems produced under accident conditions, the lighter homologue tellurium was utilized to replace it in the present research. Quantitive study and structural characterization of tellurium adsorption by Stainless steel-Ni-Cu-Ag multiple-layer mesh (SNCA) were discussed as well. The results indicated that the tellurium accumulation ascended with rising copper electroplating current density due to the increase of silver coating. The Te(IV) accumulated by naked stainless steel mesh was negligible, and the granular silver coating had a stronger adsorption ability than the flat layer after contacting for 64 h. The results suggested the high dependence of tellurium accumulation on the available surface area of silver layer. The tellurium accumulation rose at first and gone down later with the increasing of iodine ions, which resulted from the joint effects of competitive adsorption between I^- and TeO_3^{2-}, the reduction of iodine ions and the refinement of silver particles. The SEM-EDS showed a smoky tellurium precipitation formed between silver particles. Elemental mapping imaging depicted completely identical spatial distributions of silver and tellurium, revealing the selective adsorption of Te(IV) by silver. Besides, the XPS demonstrated that the spontaneous deposition of Te(IV) and the oxidation-reduction reaction between silver and Te(IV) both play important roles in removal of tellurium from aqueous solution.

© 2017 Elsevier Ltd. All rights reserved.

1. Introduction

Accelerator driven sub-critical system (ADS) has been regarded as a potential powerful tool for the treatment of nuclear waste. The development programs and researches on ADS have been launched in Russia, America, Japan (Sasa et al., 2004) and European Union (Abderrahim et al., 2010). China also initiated the ADS research project in 2011 (Wu et al., 2014a, 2015a, 2016; Wang et al., 2015) and carried out extensively studies on conceptual design (Wu and FDS Team, 2006; Wu and FDS Team, 2008; Wu et al., 2011), technical exploration (Qiu et al., 2000), application development (Wu et al., 1999, 2015b; Wu and FDS Team, 2009) and so on. The lead-bismuth eutectic (LBE) had been selected as one of the most promising coolants and spallation target materials for ADS due to its excellent neutronics, thermal-hydraulics and inherent safety characteristics (Wang et al., 2015). However, some issues should be taken into consideration with the development of LBE-cooled reactors, for instance, the isotopes of polonium that produced by proton-induced spallation reaction and neutron capture reaction on bismuth (Neuhausen et al., 2004). Polonium-210 (Po-210), which decays by emission of α particles with an energy of 5.5 MeV and a half-life of 138.38 days (Rizzi et al., 2014), is vital to be concerned for the radiation protection in LBE-cooled reactors. It would spread to aqueous solution once heat exchanger crevasse or severe nuclear meltdown accidents happen in reactors. And as we know, it can also enter into the human body through drinking water and food chain if the polluted water discharged into environmental without treatment. Po-210 would accumulate essentially in kidney, spleen and liver and then cause irreversible damage

to these organs due to their complete adsorption of the α particle energy. The maximum permissible activity of Po-210 for once human intake being regulated by the International Commission on Radiological Protection (ICRP) is only 0.74 kBq, equivalent to a particle weighing 4.5×10^{-12} g. Nevertheless, the Po-210 activity in the LBE for 15 MW target circuit after 1 year operation is estimated to be ~10^4Ci (Yefimov et al., 1997), which is 12 orders of magnitude higher than the maximum permissible intake. Therefore, in order to enhance the emergency response capability and prevent the serious radioactive pollution, it is necessary to develop an effective filter to remove polonium from radioactive wastewater. However, to our best knowledge, there are no documented works that aims at polonium removal from aqueous solution except the studies on its accumulation behavior in living organisms (Stewart and Fisher, 2003; Cherrier et al., 1995; LaRock et al., 1996; Skwarzec and Fabisiak, 2007; Carvalho and Fowler, 1993).

Tellurium (Te) is a lighter homologue of Po in chalcogen group. Even though its melting point and boiling point are somewhat higher than those of Po, it was also widely used as a surrogate in published work, such as the characteristic investigation of Po removal from liquid LBE in Buongiorno's and Ermolaev's reports (Buongiorno et al., 2004; Ermolaev et al., 1998). As indicated in the literature, the polonium in aqueous solution is mainly tetravalent (Po(IV)) (Starik et al., 1964). And Te(IV) and Po(IV) have high similarity in the chemical behavior (Ayala et al., 2012). Apart from these, the Po isotopes are radioactive and Te has non-radioactive isotopes, which can be handled more easily. Accordingly, the Te(IV) solution was used in place of Po-containing aqueous solution in this work.

With the diversified development of material, the studies on novel metals that contain hybrid nanocomposites and nanostructures have received more attention in the past few years (Xing et al., 2016a,b), especially the silver. And due to its unique properties, the silver decorated composites have been widely researched in anti-bacteria (Zhang et al., 2011a), conduction (Wu et al., 2014b), catalyst (He et al., 2012), sensing (Zhao et al., 2013; Zhan et al., 2014) and surface field enhance (Dutta et al., 2013). Besides, silver possesses good corrosion resistance and high chemical stability. Its hybrid nanocomposites are always used in wastewater treatment (Dubey et al., 2014; Fan et al., 2015; Jiao et al., 2015a). And the porous architecture is now considered to be an optimum choice because of its novel characteristics, such as large surface area, low cost and small density. For example, Tifeng Jiao's group fabricated the porous structured composite hydrogel materials of acrylic acid-AgNPs, which demonstrated good removal capacities for congo red, rhodamine B and methylene blue (Hou et al., 2016). Notably, due to the good mechanical strength, these three-dimensional porous materials could be separated from aqueous solution easily after reaction. It can be expected that the suitable silver porous material with high mechanical strength will be promising for water treatment. In our studies, 316L stainless steel mesh was selected as the supporting matrix, and the filter deposited with a porous silver layer was fabricated for Te(IV) removal. Nickel was first electroplated to avoid the oxidation of steel. And then, Copper transition layer was electroplated to enhance the adhesion between silver and the matrix. The effect of copper electroplating current density, silver deposition time, contact time and iodine ionic strength on Te(IV) adsorption by silver loaded stainless steel mesh were investigated through batch technique. The pH was fixed at 1.0 to ensure the solubility of Te(IV) in aqueous solution. To illustrate accumulated Te(IV) by SNCA and the mechanisms involved, scanning electron microscope equipped with an energy dispersive spectrometer (SEM-EDS) and X-ray photoelectron spectroscopy (XPS) were utilized.

2. Materials and methods

2.1. Preparation of silver loaded stainless steel mesh

Stainless steel meshes with diameter of 30 mm were sonicated in industrial detergent and 5 wt% sodium hydrate solution for 30 min, respectively. To remove the oxide film on the stainless steel wires, They were washed in dilute acid solution at the temperature of 60 °C for 15 min. Then, in turn, the meshes were treated in the solutions of $FeCl_3$ and H_2SO_4 to achieve a smooth and polished surface. After cleaning, Ni film was electroplated on the stainless steel meshes in aqueous solution of $NiCl_2$ at 0.21 A/dm^2, followed by electro-deposition of copper from $CuSO_4$ solution at a certain current density. The resulting meshes were pre-treated in an aqueous $AgNO_3$ solution (marked as $AgNO_3$-1) for 10 min. And then Ag layer was electroless-plated in another aqueous solution of $AgNO_3$ (marked as $AgNO_3$-2) for the desired time, in which sodium tartrate was used as reducing agent. To avoid oxidation, The obtained Stainless steel-Ni-Cu-Ag multiple-layer meshes (SNCAs) were stored in acetone for further use. The main compositions of the $AgNO_3$ -1 and $AgNO_3$-2 solutions are listed in Table 1.

2.2. Chemicals

All of the chemicals, such as sodium hydrate, hydrochloric acid (37% w/w), ferric chloride, sulphuric acid (98% w/w), nickel chloride hexahydrate, copper sulphate pentahydrate, silver nitrate, sodium sulphite, potassium dihydrogen phosphate, ammonium hydroxide (28% w/w), sodium tartrate, potassium iodide, nitric acid (68% w/w), and tellurium power (99.999% purity), were purchased from Sinopharm Chemical Reagent Co., Ltd (Shanghai, China) and were used as received. High purity deionized water (18.2 MΩ cm) obtained from an ultrapure water polishing system (Kertone, UK) was used in all experiments.

The Te(IV) solutions were prepared by dissolving the ultrafine tellurium powder in a minimum of nitric acid (Andrews and Johnson, 1976). Then, the solution was evaporated to expulse nitric acid and diluted with 1 M HCl solution to give a 1 mg/ml Te(IV) solution. The resulting stock solution of Te(IV) was progressively diluted to desired concentration and was stored below pH 1.0. And NaOH was used to adjust the pH.

2.3. Batch adsorption experiments

2.3.1. Effect of copper electroplating current density

For the SNCAs used in this experiment, the Cu film was electroplated at current densities of 0.21 A/dm^2, 0.28 A/dm^2, 0.35 A/dm^2 and 0.50 A/dm^2, respectively, and the silver was deposited on the surface of Cu coating for 1.5 h. After that, the obtained SNCAs were cast into high borosilicate glass tubes filled with 25 ml of 100 μg/ml Te(IV) at room temperature. The pH of the systems was adjusted to 1.0 with negligible volume of 5 M and 0.5 M NaOH. After contacting for 24 h, the meshes were separated and the solutions were determined for the residual tellurium. Mesh-free controls were run concurrently in all experiments to ensure that the Te(IV) accumulated on the wall of the tubes was excluded.

Table 1
The main composition of immersion silver and silver electroless plating solutions.

AgNO₃ -1 (mol/L)		AgNO₃ -2 (mol/L)	
$AgNO_3$	0.03	$AgNO_3$	0.06
Na_2SO_3	1.98	NH_4OH	0.56
KH_2PO_4	0.44	$C_4H_4Na_2O_6$	0.26

2.3.2. Effects of silver deposition time and contact time

The SNCAs deposited silver for 1.5 and 2.5 h were labelled as SNCA-1.5 and SNCA-2.5, respectively. Effect of contact time on Te(IV) adsorption by naked mesh, SNCA-1.5 and SNCA-2.5 were all conducted in the range of 0–72 h. At the desired contact time intervals, the meshes were fetched out and the residual Te(IV) was analyzed. Adsorption performance of the silver layers can be calculated by the following equation:

$$Adsorption\ (\%) = (C_o - C_t)/C_o \times 100 \tag{1}$$

where, C_o is the initial concentration of Te(IV) (mg/L) and C_t is the concentration of Te(IV) after contacting for t hours (mg/L).

2.3.3. Effect of coexisting iodine ions

The iodine ions (I^-) is one of the important radionuclides in wastewater produced in nuclear reactors. So the effect of coexisting I^- on Te(IV) adsorption by SNCA was also considered in this work. Firstly, negligible volumes of 0.1 or 0.01 M potassium iodide were added into 25 ml of 100 μg/ml Te(IV) solution, and the mixed solutions were pre-equilibrated by shaking for 30 min at ambient temperature. Then the SNCA deposited silver for 2.5 h were dropped in the mixed solution and contacted for 24 h. The following steps were the same as above copper electroplating current density investigation section.

2.4. Tellurium assay and characterization

The morphology and composition were explored by SEM-EDS on a ∑IGMA (Carl Zeiss, GER) with an accelerating voltage of 20 kV. The chemical state of silver and tellurium were studied by XPS on an ESCALAB 250 (Thermo, USA) using monochromated Al K$_\alpha$ radiation.

3. Results and discussions

3.1. Researches on influential factors

3.1.1. Effect of copper electroplating current density

Fig. 1 shows the adsorption of Te(IV) by SNCAs as a function of copper electroplating current density. For the SNCA prepared at 0.21 A/dm^2, just 8.36 ± 1.7% of Te(IV) was removed from the aqueous solution. Between 0.28 and 0.50 A/dm^2, the percentage of accumulated Te(IV) increased almost linearly, and it reached up to 35.7 ± 1.2% at 0.50 A/dm^2.
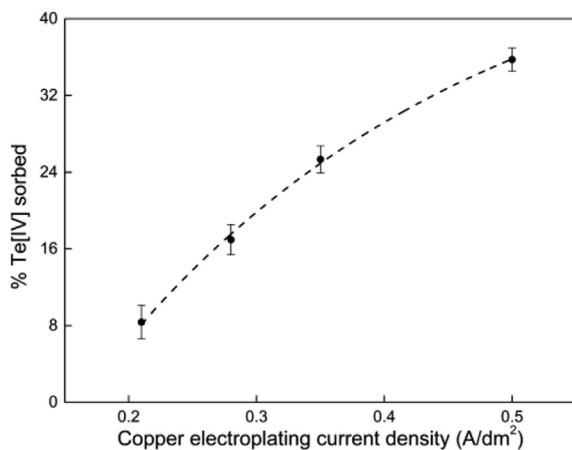
Fig. 2 displays the SEM micrographs of the tested samples. The silver particles with a size of 1–2 μm scattered on the surface of SNCA prepared at lower current density (Fig. 2a). With the increase of copper electroplating current density, the density of silver particles increased and they were connected to each other (Fig. 2b). When the current density increased to 0.35 A/dm^2, an intact silver coating was available. And owing to the continuous deposition of silver, a compact granulated silver layer formed as the current density further raised to 0.50 A/dm^2. The approximate percentage content of silver and tellurium attached on the SNCAs were also analyzed before and after adsorption. As shown in Fig. 3, the average weight percentage of the silver ascends from 34.1 ± 1.4 to 79.6 ± 0.9 wt% in the range of 0.21–0.50 A/dm^2. After adsorption, the content of tellurium on SNCAs also present a similar rising trend, and it reached up to 20.5 ± 0.5 wt % at 0.50 A/dm^2. According to the above analysis result, it can be inferred that the increase of accumulated Te(IV) with increased copper electroplating current density resulted from the enhancement of available silver on the SNCAs. In a follow-up experiment, 0.50 A/dm^2 was selected as the current density of copper electroplating for sample preparation.

3.1.2. Effect of silver deposition time and contact time

Fig. 4 demonstrates the contact time dependent Te(IV) accumulation on the SNCA-1.5, SNCA-2.5 and naked stainless steel
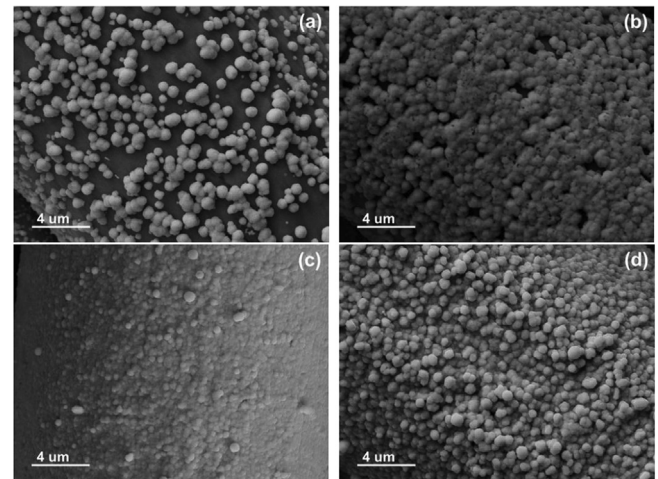

Fig. 2. SEM micrographs of SNCAs prepared at copper electroplating current densities of 0.21 A/dm^2 (a), 0.28 A/dm^2 (b), 0.35 A/dm^2 (c) and 0.50 A/dm^2 (d).

Fig. 1. Tellurium accumulated on SNCAs prepared at different copper electroplating current density.
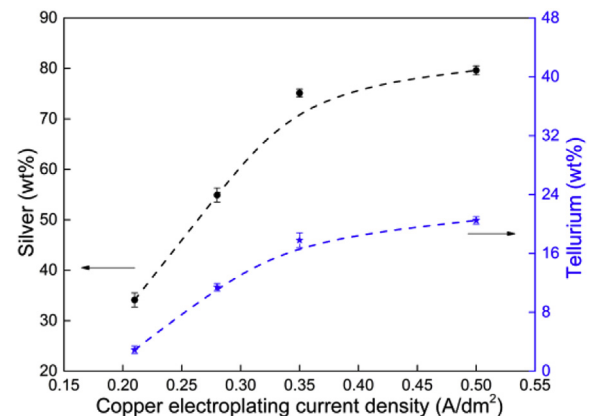

Fig. 3. The weight percentage of the silver and tellurium attached on the SNCAs prepared at different copper electroplating current densities.
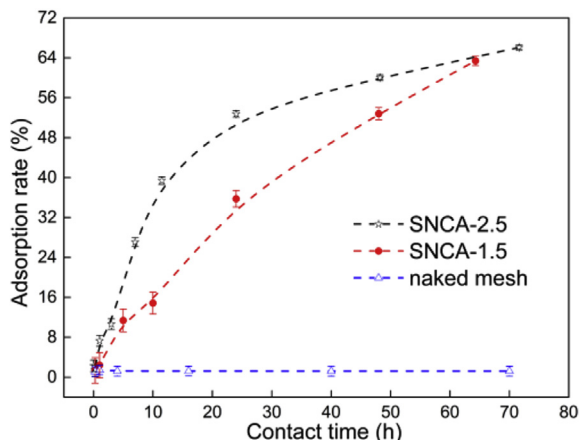
Fig. 4. Effects of contact time and silver deposition time on Te(IV) adsorption by SNCAs and naked meshes.

meshes. There was no Te(IV) removed from aqueous solution by the naked meshes in the range of 0–72 h. The kinetics of Te(IV) accumulation on SNCA-2.5 can be divided by two periods. In the first 11 h, the percentage of accumulated Te(IV) rose at constant rates and around 40% of Te(IV) was removed from the aqueous solution. It is also evident that the rise speed of SNCA-2.5 was significantly higher than SNCA-1.5 in this phase. Then, the Te(IV) adsorption by SNCA-2.5 entered the second phase. The climbing trend of SNCA-2.5 slowed down obviously and increased at a much lower rate over the next hours. However, unlike the SNCA-2.5, the percentage of accumulated Te(IV) grew about linearly in the same time frame. After contacting for 64 h, the percentages of Te(IV) accumulation reached to $63.4 \pm 0.1\%$, which was basically the same as SNCA-2.5.

The SEM micrographs and the EDS line scanning analysis on the cross-sections of the SNCA-1.5 and the SNCA-2.5 were present in

Fig. 5. The thickness of the silver layer on SNCA-2.5 was about 3 μm (Fig. 5b), which was one and a half times more than the SNCA-1.5 (Fig. 5a). This would be the main reason for Te(IV) quick adsorption by SNCA-2.5 in the first stage. But with prolonging the contact time, multilayer formation by the tellurium accumulation on the surface of silver coating tended to prevent the attachment of tellurium, which decreased the adsorption rate of the silver layer. The angular-grained silver layer (Fig. 5c), possessing both the external surface and the internal surface, can offer more contact area for Te(IV) adsorption. It would be the main cause for the continuous ascent of Te(IV) accumulation on SNCA-1.5 in the adsorption process. The superficial surface of the silver layer was accessible for Te(IV) ions. It mainly played a role in the initial stage. The inner surface between particles, which was less likely to contact with a large quantity of Te(IV) ions soon, would work later. Based on the above, one can draw a conclusion that the adsorption kinetics of SNCAs was highly depending on the surface area of the silver coating. To obtain a higher accumulation capacity in a relatively short term, 2.5 h was identified as the time of silver deposition and 24 h was selected as contact time in the subsequent experiment.

3.1.3. Effect of coexisting iodine ions

The effect of iodine ions on Te(IV) adsorption by SNCA was also investigated. As shown in Fig. 6, the percentage of accumulated Te(IV) descends dramatically within the concentration range of $0–3.8 \times 10^{-5}$ mol/L and reaches the bottom at $20.3 \pm 0.4\%$. The speciation of Te(IV) strongly depends on the pH heavily. At pH 1.0, the prominent species is reported to be TeO_3^{2-} (Maskaeva et al., 2012). The experimental phenomenon indicated a competition between the I^- and TeO_3^{2-}. As the concentration of iodine ions increased, the Te(IV) accumulation on SNCA ascended and returned back to $57.7 \pm 0.4\%$ at iodine concentration of 6×10^{-4} mol/L. Meanwhile, the SNCAs exposed to the mixed solution of I^- and Te(IV) were also observed to be somber black streaked with green.
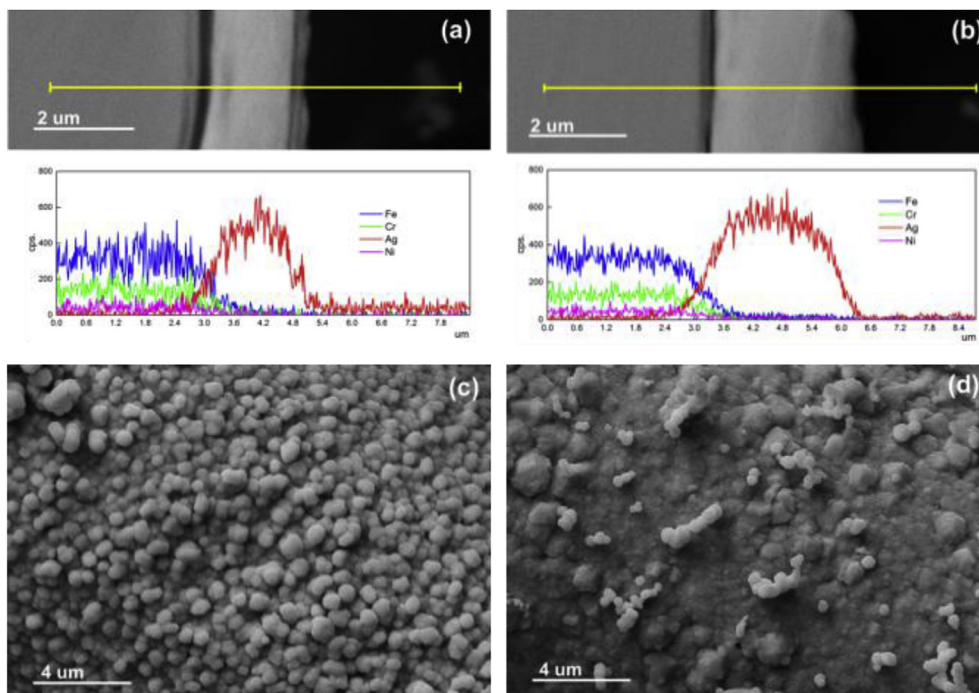

Fig. 5. Cross-section (above) and appearance (below) analysis of silver cladding on stainless steel mesh deposited silver for 1.5 h (a, c) and 2.5 h (b, d).
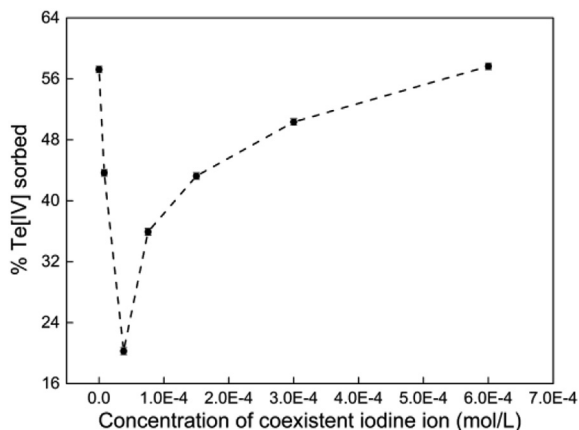
Fig. 6. Effect of coexisting iodine ions on Te(IV) adsorption by SNCA-2.5.

variation with increasing concentration of I⁻ indicated that, the higher the I⁻ level in the aqueous solution was, the more thoroughly the reaction went on. The synthetic action of the intensified silver surface area and the eased competitive adsorption between the TeO_3^{2-} and I⁻ leads to the enhancement of Te (IV) accumulation at higher concentration of iodine ions.

3.2. Characterizations and analysis

Fig. 7a displays the SEM micrograph of SNCA-2.5 in control experiment. Compared with Fig. 5c, there was no obvious change was observed after treating in acidic solutions that had no Te(IV). Fig. 7b shows the images of SNCA-2.5 after adsorption. An enveloping substance different from stainless steel substrate appeared between silver particles, suggesting the occurrence of tellurium accumulation on silver loaded stainless steel mesh. In addition, structure fracture of silver layer caused in the process of Te(IV) accumulation was also observed. Energy dispersive X-ray analysis of the white squares confirmed the deposition of tellurium on the silver layer evidently. The spectra exhibited marked peaks of silver. After adsorption, the distinct peaks of tellurium were displayed (Fig. 7c).

The elemental mapping images of a specific spot scraped before adsorption was shown in Fig. 8. The spatial distribution of tellurium on the surface of SNCA was completely contrary to that of iron, chromium and nickel, but consistent with that of silver. The distributed intensity of tellurium increased correspondingly in the region with high silver content, indicating the selective adsorption of Te(IV) from acid solution by the silver layer. It agrees with Karali's results (Karali et al., 1996), in which silver was observed to possess outstanding spontaneous deposition efficiency for polonium.

More detailed information regarding the chemical variation of Te(IV) and Ag before and after adsorption were identified using X-
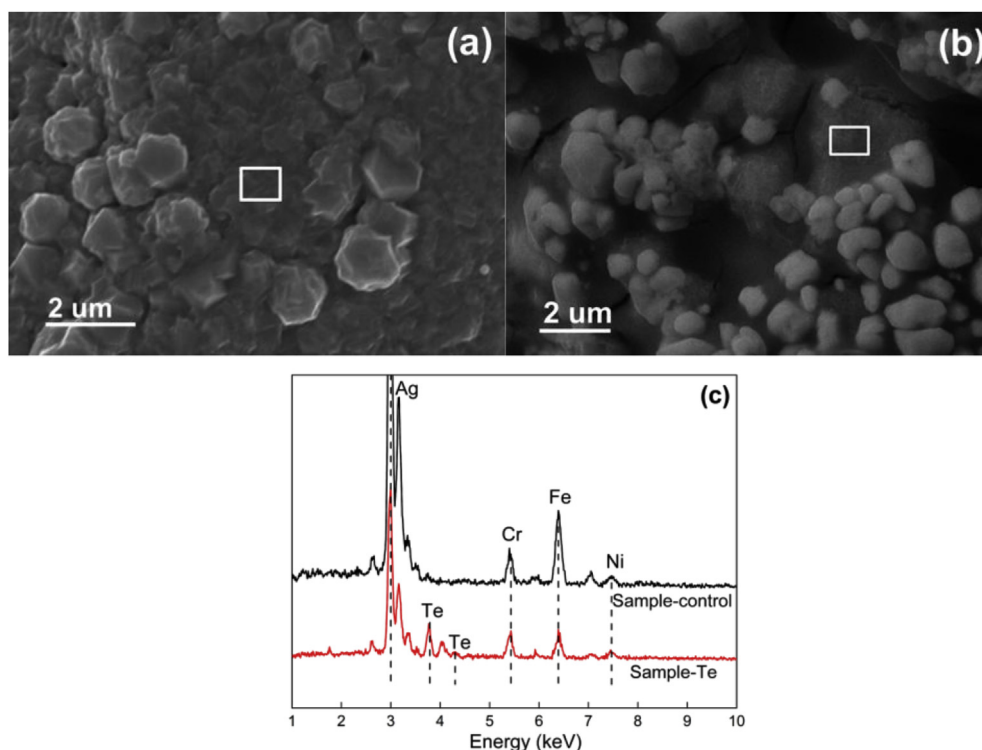
And the colour was deepened apparently as the iodine concentration increased from 3.8×10^{-5} to 6×10^{-4} mol/L. The distinct characteristic indicated the formation of AgI and its decomposition in the light. The whole reaction process can be described as follows.

$$Ag \leftrightarrow Ag^+ + e^- \tag{2}$$

$$Ag^+ + I^- \rightarrow AgI\downarrow \tag{3}$$

$$AgI \xrightarrow{light} Ag + I_2\uparrow \tag{4}$$

As a result of these reactions, silver layer transformed to the one consisted of ultra-fine particles. And the I⁻ in aqueous solution decreased due to the volatilization of the formed I_2. The colour

Fig. 7. SEM micrographs of SNCA-2.5 treated in acidic solution (a) and exposed to Te(IV) (b) and the EDS analysis of the white squares (c).
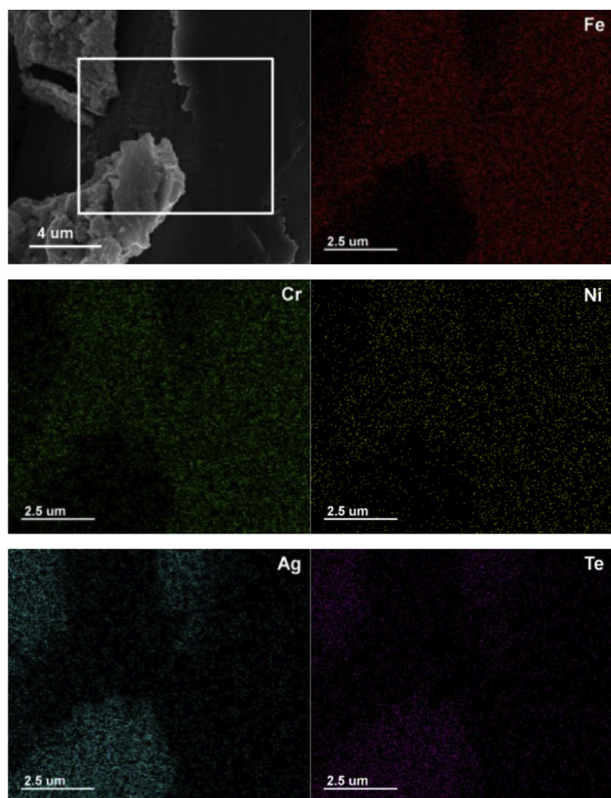
Fig. 8. Elemental mapping characterization of SNCA exposed to Te(IV) for 24 h.

ray photoelectron spectroscopy. Fig. 9a shows the overall spectra of Te(IV) stock solution (noted as Te), SNCA and SNCA contacted with Te(IV) (noted as SNCA—Te) in the range of 0—1000 eV. The spectral line of C 1s (284.6 eV) was utilized to calibrate the binding energies. The peaks of Te and Ag just appeared in the spectra of SNCA and Te, respectively. But after exposed to Te(IV) for 24 h, both of them were exhibited in the spectra of SNCA—Te. A detailed deconvolution of the Ag 3d peak was performed after a Shirley background subtraction for SNCA and SNCA-Te. The results were shown in Fig. 9b. The peaks of Ag $3d_{3/2}$ and Ag $3d_{5/2}$ were respectively observed at binding energies of about 374.2 and 368.2 eV in both spectra (Zhan et al., 2014; Zhang et al., 2011a,b). The slitting of the 3d doublet of Ag is 6.0 eV, suggesting the metallic nature of silver (Zhang et al., 2011a,b; Jiao et al., 2015b). In addition, there were two new peaks appeared at 374.1 and 368.1 eV in high —resolution Ag 3d XPS spectrum of SNCA-Te, which can be ascribed to Ag(I) 3d binding energies (Zuo et al., 2008). Fig. 9c shows that the peaks located at 587.7 ± 0.2 and 577.3 ± 0.2 eV correspond to Te(IV) $3d_{3/2}$ and Te(IV) $3d_{3/2}$ binding energies (Bahl et al., 1977; Zhou et al., 2002; Xiao et al., 2010), which illustrated the spontaneous deposition of Te(IV) on silver. Interestingly, two small peaks also appeared at 582.7 ± 0.2 and 572.4 ± 0.2 eV with a broad slitting of 10.3 eV in the SNCA—Te spectrum.

Spectrum. Binding energies of the Te(II-) $3d_{5/2}$ levels lie typically between 572.2 and 573.3 eV (Xiao et al., 2010; Jiang et al., 2001; Dong and Zhu, 2012). Combine with the XPS analysis results of Ag, it can be speculated that a substantial part of metallic silver reacted with Te(IV) to form Ag_2Te on the surface of silver layer (Zuo et al., 2008; Jiang et al., 2001). In this sense, the spontaneous deposition and the chemical bonding both take important roles in Te(IV) adsorption by porous silver layer.
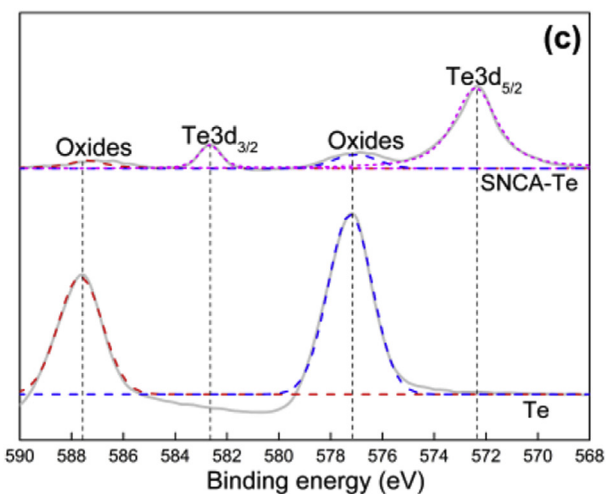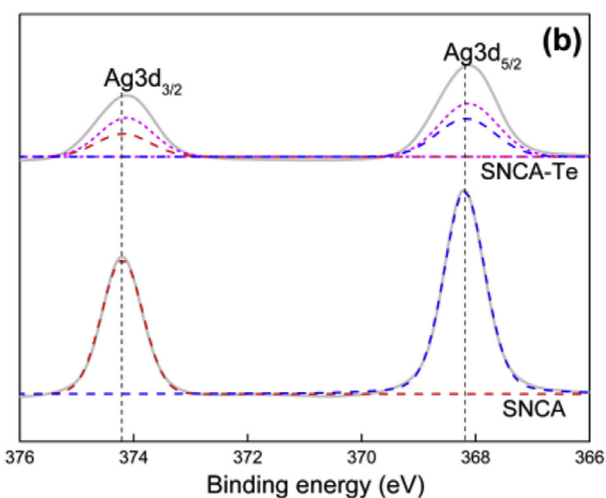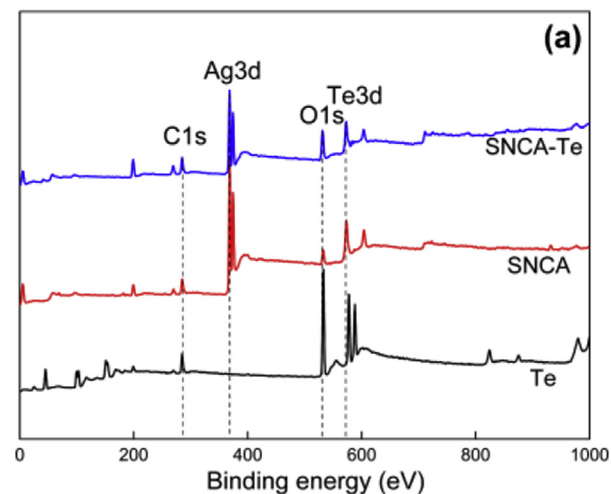

Fig. 9. XPS characterizations of tellurium stock solution and SNCA before and after adsorption.

4. Conclusions

A novel kind of mesh loaded with porous silver layer was prepared, characterized and utilized as filter for Te(IV) removal from aqueous solution. The effects of copper electroplating current density, silver deposition time, contact time, and iodine ionic strength were first studied. The percentage of Te(IV) accumulation on SNCAs increased with increasing copper electroplating current density as more silver was available. The Te(IV) accumulated by SNCA-1.5 was relatively slower in the first 11 h and it achieved as much as SNCA-2.5 at the end of adsorption as a result of the large surface area of silver coating. There was a competitive reaction existing between iodine ions and Te(IV) ions. But the Te(IV) accumulation enhanced in the surrounding of higher iodine concentrations due to the significant decrease of iodine level and the refinement of silver particles. The SEM-EDS, Elemental mapping and XPS analysis of SNCAs before and after adsorption revealed that the spontaneous deposition of Te(IV) and chemical reaction between silver and Te(IV) were two main mechanisms involved in the selective adsorption of Te(IV) on silver layer. The silver loaded stainless steel mesh, fabricated by the very simple manner and convenient to separate, possesses extensive adsorption ability for the tellurium. It is a promising alternative filter for removing polonium from acidic radioactive wastewater.

Acknowledgements

References

Abderrahim, H.A., Baeten, P., De Bruyn, D., Heyse, J., Schuurmans, P., Wagemans, J., 2010. MYRRHA, a multipurpose hybrid research reactor for high-end applications. Nucl. Phys. News 20 (1), 24–28.

Andrews, R.W., Johnson, D.C., 1976. Determination of selenium(IV) by anodic stripping voltammetry in flow system with ion exchange separation. Anal. Chem. 48 (7), 1056–1060.

Ayala, R., Martínez, J.M., Pappalardo, R.R., Sánchez Marcos, E., 2012. Quantum-mechanical study on the aquaions and hydrolyzed species of Po(IV), Te(IV), and Bi(III) in water. J. Phys. Chem. B 116 (51), 14903–14914.

Bahl, M.K., Watson, R.L., Irgolic, K.J., 1977. X-ray photoemission studies of tellurium and some of its compounds. J. Chem. Phys. 66 (12), 5526–5535.

Buongiorno, J., Loewen, E.P., Czerwinski, K., Larson, C., 2004. Studies of polonium removal from molten lead-bismuth for lead-alloy-cooled reactor applications. Nucl. Technol. 147 (3), 406–417.

Carvalho, F.P., Fowler, S.W., 1993. An experimental study on the bioaccumulation and turnover of polonium-210 and lead-210 in marine shrimp. Mar. Ecol. Prog. Ser. 102 (1), 125–133.

Cherrier, J., Burnett, W.C., LaRock, P.A., 1995. Uptake of polonium and sulfur by bacteria. Geomicrobiol. J. 13 (2), 103–115.

Dong, G.H., Zhu, Y.J., 2012. One-step microwave-solvothermal rapid synthesis of Sb doped PbTe/Ag2Te core/shell composite nanocubes. Chem. Eng. J. 193, 227–233.

Dutta, S., Ray, C., Sarkar, S., Pradhan, M., Negishi, Y.C., Pal, T., 2013. Silver nanoparticle decorated reduced graphene oxide (rGO) nanosheet: a platform for SERS based low-level detection of uranyl ion. ACS Appl. Mater. Interfaces 5 (17), 8724–8732.

Dubey, S.P., Dwivedi, A.D., Kim, I.-C., Sillanpaa, M., Kwon, Y.-N., Lee, C., 2014. Synthesis of graphene-carbon sphere hybrid aerogel with silver nanoparticles and its catalytic and adsorption applications. Chem. Eng. J. 244, 160–167.

Ermolaev, N., Bugreev, M., Yefimov, E., 1998. Methods of removal and containment of radioactive polonium from lead-bismuth coolant. Proc. Heavy Liq. Metal Cool. Nucl. Technol 1, 194–200 (HLMC-98).

Fan, Y.Y., Ma, W.G., Han, D.X., Gan, S.Y., Dong, X.D., Niu, L., 2015. Convenient recycling of 3D AgX/graphene aerodels (X=Br, Cl) for efficient photocatalytic degradation of water pollutants. Adv. Mater. 27 (25), 3767–3773.

He, Y.Q., Zhang, N.N., Gong, Q.J., Li, Z.L., Gao, J.P., Qiu, H.X., 2012. Metal nanoparticles supported graphene oxide 3D porous monoliths and their excellent catalytic activity. Mater. Chem. Phys. 134 (2–3), 585–589.

Hou, C.L., Ma, K., Jiao, T.F., Xing, R.R., Li, K.K., Zhou, J.X., Zhang, L.X., 2016. Preparation and dye removal capacities of porous silver nanoparticle-containing composite hydrogels via poly (acrylic acid) and silver ions. RSC Adv. 6 (112), 110799–110807.

Jiang, Y., Wu, Y., Yang, Z.P., Xie, Y., Qian, Y.T., 2001. Room temperature growth of rod-like nanocrystalline Ag2Te in mixed solvent. J. Cryst. Growth 224 (1–2), 1–4.

Jiao, T.F., Guo, H.Y., Zhang, Q.R., Peng, Q.M., Tang, Y.F., Yan, X.H., Li, B.B., 2015b. Reduced graphene oxide-based silver nanoparticle-containing composite hydrogel as highly efficient dye catalysts for wastewater treatment. Sci. Rep. 5, 11873.

Jiao, T.F., Zhao, H., Zhou, J.X., Zhang, Q.R., Luo, X.N., Hu, J., Peng, Q.M., Yan, X., 2015a. Self-Assembly reduced graphene oxide nanosheet hydrogel fabrication by anchorage of chitosan/silver and its potential efficient application toward dye degradation for wastewater treatments. ACS Sustain. Chem. Eng. 3 (12), 3130–3139.

Karali, T., Ölmez, S., Yener, G., 1996. Study of spontaneous deposition of 210 Po on various metals and application for activity assessment in cigarette smoke. Appl. Radiat. Isot. 47 (4), 409–411.

LaRock, P.A., Hyun, J.H., Boutelle, S., Burnett, W.C., Hull, C.D., 1996. Bacterial mobilization of polonium. Geochim. Cosmochim. Acta 60 (22), 4321–4328.

Maskaeva, L.N., Vovkotrub, E.G., Markov, V.F., 2012. Conditions of hydrochemical synthesis, composition, and structure of tellurium films. Russ. J. Appl. Chem. 85 (5), 731–735.

Neuhausen, J., Köster, U., Eichler, B., 2004. Investigation of evaporation characteristics of polonium and its lighter homologues selenium and tellurium from liquid Pb-Bi-eutecticum. Radiochim. Acta 92 (12/2004), 917–923.

Qiu, L.J., Wu, Y.C., Xiao, B.J., Xu, Q., Huang, Q.Y., Wu, B., Chen, Y.X., Xu, W.N., Chen, Y.P., Liu, X.P., 2000. A low aspect ratio tokamak transmutation system. Nucl. Fusion 40 (3Y), 629–633.

Rizzi, M., Neuhausen, J., Eichler, R., Türler, A., Mendonca, T.M., Stora, T., Gonzalez Prieto, B., Aerts, A., Schumann, D., 2014. Polonium evaporation from dilute liquid metal solutions. J. Nucl. Mater. 450 (1–3), 304–313.

Sasa, T., Oigawa, H., Tsujimoto, K., Nishihara, K., Kikuchi, K., Kurata, Y., Saito, S., Futakawa, M., Umeno, M., Ouchi, N., Arai, Y., Minato, K., Takano, H., 2004. Research and development on accelerator-driven transmutation system at JAERI. Nucl. Eng. Des. 230 (1), 209–222.

Skwarzec, B., Fabisiak, J., 2007. Bioaccumulation of polonium 210Po in marine birds. J. Environ. Radioact. 93 (2), 119–126.

Starik, I.E., Ampelogova, N.I., Kuznetsov, B.S., 1964. Hydrolysis of polonium in PERCHLORIC acid. Radiokhimiya 6, 519–524.

Stewart, G.M., Fisher, N.S., 2003. Experimental studies on the accumulation of polonium-210 by marine phytoplankton. Limnol. Oceanogr. 48 (3), 1193–1201.

Wang, M.H., Lian, C., Li, Y.Y., Wang, D., Jie, J.Q., Wu, Y.C., 2015. Preliminary conceptual design of a lead–bismuth cooled small reactor (CLEAR-SR). Int. J. Hydrogen Energy 40 (44), 15132–15136.

Wu, Y.C., Bai, Y.Q., Song, Y., Huang, Q.Y., Zhao, Z.M., 2016. Development strategy and conceptual design of China lead-based research reactor. Ann. Nucl. Energy 87 (Part 2), 511–516.

Wu, Y.C., Bai, Y.Q., Song, Y., Huang, Q.Y., Lian, C., Wang, M.H., Zhou, T., Jin, M., Wu, Q.S., Wang, J.Y., Jiang, J.Q., Hu, L.Q., Li, C.J., Gao, S., Li, Y.Z., Long, P.C., Zhao, Z.M., Yu, J., FDS Team, 2014a. Conceptual design of China lead-based research reactor CLEAR-I. Nucl. Sci. Eng. 34 (02), 201–208 ([in Chinese]).

Wu, C., Fang, L.J., Huang, X.Y., Jiang, P.K., 2014b. Three-dimensional highly conductive graphene–silver nanowire hybrid foams for flexible and stretchable conductors. ACS Appl. Mater. Interfaces 6 (23), 21026–21034.

Wu, Y.C., FDS Team, 2006. Conceptual design activities of FDS series fusion power plants in China. Fusion Eng. Des. 81 (23), 2713–2718.

Wu, Y.C., FDS Team, 2008. Conceptual design of the China fusion power plant FDS-II. Fusion Eng. Des. 83 (10), 1683–1689.

Wu, Y.C., FDS Team, 2009. CAD-based interface programs for fusion neutron transport simulation. Fusion Eng. Des. 84 (7), 1987–1992.

Wu, Y.C., Jiang, J.Q., Wang, M.H., Jin, M., FDS Team, 2011. A fusion-driven subcritical system concept based on viable technologies. Nucl. Fusion 51 (10), 103036–103042.

Wu, Y.C., Song, J., Zheng, H.Q., Sun, G.Y., Hao, L.J., Long, P.C., Hu, L.Q., FDS Team, 2015a. CAD-based Monte Carlo program for integrated simulation of nuclear system SuperMC. Ann. Nucl. Energy 82, 161–168.

Wu, Y.C., Wang, M.H., Huang, Q.Y., Zhao, Z.M., Hu, L.Q., Song, Y., Jiang, J.Q., Li, C.J., Long, P.C., Bai, Y.Q., Lian, C., Zhou, T., Jin, M., FDS Team, 2015b. Development status and prospects of lead-based reactors. Nucl. Sci. Eng. 35 (02), 213–221 (in Chinese).

Wu, Y.C., Xie, Z.S., Ulrich, F., 1999. A discrete ordinates nodal method for one-dimensional neutron transport calculation in curvilinear geometries. Nucl. Sci. Eng. 133 (3), 350–357.

Xiao, F., Chen, G., Wang, Q., Wang, L., Pei, J., Zhou, N., 2010. Simple synthesis of ultra-long Ag 2 Te nanowires through solvothermal co-reduction method. J. Solid State Chem. 183 (10), 2382–2388.

Xing, R.R., Jiao, T.F., Liu, Y.M., Ma, K., Zou, Q.L., Ma, G.H., Yan, X.H., 2016a. Co-assembly of graphene oxide and albumin/photosensitizer nanohybrids towards enhanced photodynamic therapy. Polymers 8 (5), 181.

Xing, R.R., Liu, K., Jiao, T.F., Zhang, N., Ma, K., Zhang, R.Y., Zou, Q.L., Ma, G.H., Yan, X.H., 2016b. An injectable self-assembling collagen–gold hybrid hydrogel for combinatorial antitumor photothermal/photodynamic therapy. Adv. Mater. 28 (19), 3669–3676.

Yefimov, E.I., Pankratov, D.V., Ignatiev, S.V., 1997. Removal and containment of high-level radioactive polonium from liquid lead-bismuth coolant. In: MRS Proceedings. Cambridge Univ Press.

Zhan, B.B., Liu, C.B., Shi, H.X., Li, C., Wang, L.H., Huang, W., Dong, X.C., 2014.

A hydrogen peroxide electrochemical sensor based on silver nanoparticles decorated three-dimensional graphene. Appl. Phys. Lett. 104 (24), 243704.

Zhang, D.H., Liu, X.H., Wang, X., 2011a. Green synthesis of graphene oxide sheets decorated by silver nanoprisms and their anti-bacterial properties. J. Inorg. Biochem. 105 (9), 1181—1186.

Zhang, P., Shao, C.L., Zhang, Z.Y., Zhang, M.Y., Mu, J.B., Guo, Z.C., 2011b. In situ assembly of well-dispersed Ag nanoparticles (AgNPs) on electrospun carbon nanofibers (CNFs) for catalytic reduction of 4-nitrophenol. Nanoscale 3 (8), 3357—3363.

Zhao, B., Liu, Z.R., Fu, W.Y., Yang, H.B., 2013. Construction of 3D electrochemically reduced graphene oxide—silver nanocomposite film and application as nonenzymatic hydrogen peroxide sensor. Electrochem. Commun. 27, 1—4.

Zhou, W.P., Kibler, L.A., Kolb, D.M., 2002. Evidence for a change in valence state for tellurium adsorbed on a Pt(111) electrode. Electrochim. Acta 47 (28), 4501—4510.

Zuo, P.F., Zhang, S.G., Jin, B.K., Tian, Y.P., Yang, J.X., 2008. Rapid synthesis and electrochemical property of Ag2Te nanorods. J. Phys. Chem. C 112 (38), 14825—14829.